Radical-lanthanide ferromagnetic interaction in a Tb^{III} bis-phthalocyaninato complex

Dorsa Komijani, Alberto Ghirri, Claudio Bonizzoni, Svetlana Klyatskaya, Eufemio Moreno-Pineda, Mario Ruben, Alessandro Soncini, Marco Affronte, and Stephen Hill

Phys. Rev. Materials **2**, 024405 — Published 23 February 2018

DOI: 10.1103/PhysRevMaterials.2.024405

Radical-Lanthanide Ferromagnetic Interaction in a Tb^{III} Bis-Phthalocyaninato Complex

Dorsa Komijani,[1,2] Alberto Ghirri,[3] Claudio Bonizzoni,[3,4] Svetlana Klyatskaya,[5] Eufemio Moreno-Pineda,[5] Mario Ruben,[5] Alessandro Soncini,[6] Marco Affronte,[3,4,*] and Stephen Hill[1,2,*]

[1]*Department of Physics, Florida State University*, *Tallahassee, FL 32306, USA*

[2]*National High Magnetic Field Laboratory, Tallahassee, FL 32310, USA*

[3]*CNR-Instituto Nanoscienze, via G. Campi 213A, 41125 Modena, Italy*

[4]*Dipartimento di Scienze Fisiche, Informatiche e Matematiche, Università di Modena e Reggio Emilia, via G. Campi 213A, 41125 Modena, Italy*

[5]*Karlsruhe Institute of Technology (KIT), Institute of Nanotechnology, Eggenstein-Leopoldshafen, Germany*

[6]*School of Chemistry, The University of Melbourne, 3010 Victoria, Australia*

ABSTRACT

Recent studies have highlighted the importance of organic ligands in the field of molecular spintronics, via which delocalized electron spin density can mediate magnetic coupling to otherwise localized 4*f* moments of lanthanide ions, which show tremendous potential for single-molecule device applications. To this end, high-field/high-frequency electron paramagnetic resonance (EPR) spectroscopy is employed to study a neutral terbium bis-phthtalocyaninato metalorganic complex, $[TbPc_2]^0$, with the aim of understanding the magnetic interaction between the Ising-like moment of the lanthanide ion and the unpaired spin density on the coordinating organic radical ligand. The measurements were performed on a previously unknown $[TbPc_2]^0$ structural phase crystallizing in the *Pnma* space group. EPR measurements on powder samples of $[TbPc_2]^0$ reveal an anisotropic spectrum, which is attributed to the spin-½ radical coupled weakly to the EPR-silent Tb^{III} ion. Extensive double-axis rotation studies on a single-crystal reveal two independent spin-½ signals with differently oriented (albeit identical) uniaxial *g*-tensors, in complete agreement with x-ray structural studies that indicate two molecular orientations within the unit cell. The easy-axis nature of the radical EPR spectra thus reflects the coupling to the Ising-like Tb^{III} moment. This is corroborated by studies of the isostructural $[YPc_2]^0$ analog (where Y is non-magnetic yttrium), which gives a completely isotropic radical EPR signal. The

experimental results for the terbium complex are well explained on the basis of an effective model that introduces a weak ferromagnetic Heisenberg coupling between an isotropic spin-½ and an anisotropic spin-orbital moment, $J = 6$, that mimics the known, strong easy-axis Tb···Pc_2 crystal-field interaction.

I. INTRODUCTION

The study of electron delocalization involving spin-bearing (radical) ligands coordinated to metal ions is relevant to a wide range of research topics, including organic electronics, photovoltaics, and catalysis, as well as a many important biological processes and biomedical applications.[1-4] This subject also became of interest within the molecular magnetism and nanomagnetism communities, given the demonstration that radical-bearing ligands can mediate strong exchange interactions between otherwise magnetically isolated lanthanide (Ln) ions, resulting in a leap forward in the development of spin-chain systems[5-7] and so-called single-molecule magnets (SMMs)[8-10] – molecules that can be magnetized below a characteristic blocking temperature, T_B. More recently, it has been recognized that delocalized electrons in organic radicals play a key role in mediating coupling between lanthanide magnetic moments and magnetic surfaces,[11,12] or to conduction electrons in spintronic devices.[13,14] Moreover, charge transport through organic ligands provides a means of addressing electron and nuclear quantum states associated with lanthanide qubits integrated into single-molecule spin transistors.[15-17]

Although electron paramagnetic resonance (EPR) investigations have previously been employed to study Ln-radical systems,[18,19] transitions are typically silent or forbidden at the low microwave frequencies of commercial EPR spectrometers; this is due primarily to the large moment and strong crystal field anisotropy of most lanthanides, resulting in an Ising-type coupling to the radical and appreciable zero-field gaps associated with allowed magnetic dipole transitions. Consequently, the few EPR investigations targeted directly at understanding Ln-radical interactions have been performed on homebuilt high-field instruments.[20,21] Motivated by the potential use of Tb^{III}-bisphthalocyaninato ($TbPc_2$) sandwich complexes in spintronic devices, quantum information processing applications, as well as for magnetic interfaces, we set out to explore whether the magnetic properties of the highly anisotropic and sizeable Tb^{III} moment can be probed via its coupling to a nearby radical through the use of high-frequency microwave techniques. To this end, we report single-crystal and powder high-field EPR (HF-EPR)

measurements on a neutral $[TbPc_2]^0$ complex for which the organic bisphthalocyaninato ligand is open shell, i.e., it carries an unpaired electron. A highly anisotropic EPR signal can be attributed to the radical, suggesting an appreciable interaction with the Ising-like Tb^{III} ion.

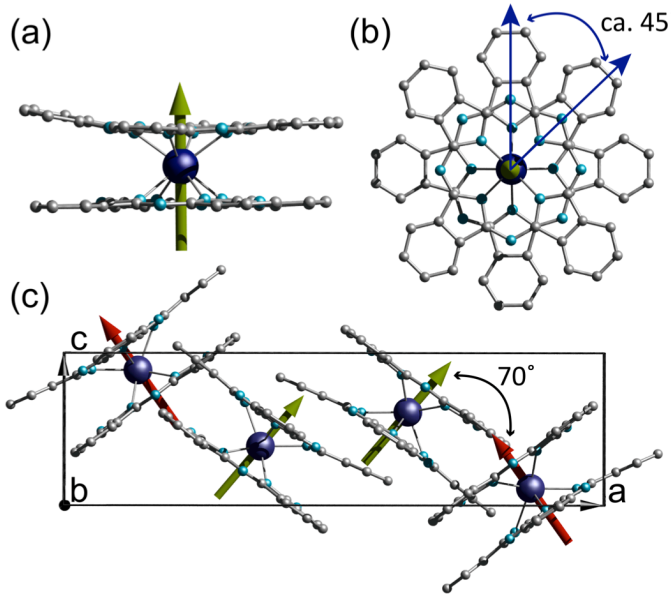

Fig. 1. Molecular structure and packing of $[TbPc_2]^0$: (a) side view; (b) top view; and (c) packing diagram of the molecules in the unit cell, displaying two magnetically inequivalent sets of molecules with their easy-axes (red/green arrows) tilted approximately 70° with respect to each other. Color scheme: Tb, purple; N, blue; C, gray; H atoms have been omitted for clarity.

As reported by Ishikawa et al. in 2003,[22] the organometallic $[TBA]^+[LnPc_2]^-$ complex [Ln = Tb, Dy, and $TBA^+ = N(C_4H_9)_4^+$] was the first example of a SMM containing just a single metal ion, in this case sandwiched between the two organic Pc ligands. Oxidation of $[Tb(Pc)_2]^-$ results in $[TbPc_2]^0$ (**1**), a neutral complex with an unpaired electron now delocalized over the two Pc rings (Fig. 1).[23] The Tb^{III} ion has a spin-orbit coupled angular momentum ground state of $J = 6$ ($L = 3$, $S = 3$), with the lowest (approximately degenerate) substates as $m_J = \pm 6$ derived on the basis of fits to ^1H NMR paramagnetic shifts and temperature dependent magnetic susceptibility.[24] The easy-axis of the terbium ion is defined by the C_4 symmetry axis of the molecule, i.e., perpendicular to the planes of the Pc rings [Fig. 1(a)]. Meanwhile, the next excited states ($m_J = \pm 5$) lie more than 400 cm^{-1} above the $m_J = \pm 6$ states and are, thus, not populated at low temperatures.[24] This large separation between the $m_J = \pm 6$ and ± 5 substates is a direct consequence of the strong axial nature of the crystal field imposed by the Pc_2 ligands on the non-spherical 4*f* electron density associated with the Tb^{III} ion. This, in turn, results in highly pure $m_J = \pm 6$ states (tunnel splitting ~kHz).[25] Thus, in contrast to recent studies of a similar Ho^{III}

compound with a 4*f* electron density that is closer to spherical (tunnel splitting ~K),[26] EPR transitions between the ground substates in **1** cannot be observed directly via EPR. However, the unpaired spin on the ligand provides an indirect way to spectroscopically probe the Tb^{III} ion and its coupling to the radical.

II. EXPERIMENTAL DETAILS

The investigated complexes, $[TbPc_2]^0$ (**1**) and isostructural $[YPc_2]^0$ (**2**), where Y is non magnetic, were synthesized according to previously established procedures.[27] Continuous wave (CW) HF-EPR measurements were first performed at low temperatures on a finely ground powder of **1** and **2** in the frequency range from 52 to 412 GHz. A transmission-type spectrometer was employed for these purposes in which microwaves are propagated through cylindrical light pipes into (and out of) a variable flow He cryostat situated within the bore of a 15/17 T superconducting magnet.[28] Microwaves were generated using a phase-locked Virginia Diode source operating at a base frequency of 12-14 GHz followed by a chain of multipliers. The returned microwave signal was recorded using magnetic field modulation and a liquid He cooled InSb Bolometer. The fine powders were pressed into polyethylene cups using a Teflon stopper to prevent mobilization in the presence of the externally applied magnetic field.

Single-crystal measurements were carried out on **1** using a cavity perturbation technique, employing a millimeter-wave vector network analyzer (MVNA) in combination with various microwave sources and detectors.[29,30] Field-swept HF-EPR spectra were recorded in a 9-5-1 T superconducting vector magnet, at fixed frequencies in the 50 to 104 GHz range. A variable-flow He gas cryostat was again used for temperature control. A single needle shaped crystal (approximate dimensions $1.5 \times 0.4 \times 0.4$ mm^3) was selected for study, and subsequently mounted horizontally on the base plate of a vertical cylindrical resonator. Due to the low-symmetry space group of **1** (see below), the unit cell axes do not project in a simple way onto the crystal shape. Consequently, extensive angle-dependent studies were first performed via *in situ* double-axis rotation: the 9-5 T component of the vector field was employed to rotate the applied field in the polar angle, θ, in 10^o increments ($\theta = 0^o$ corresponds to the field being parallel to the vertical cylindrical axis of the resonator); meanwhile, the azimuthal angle, ϕ, was varied in 20^o increments by physically rotating the resonator about its cylindrical axis. EPR spectra were then recorded at 65.5 GHz and 2 K over a 180^o range in θ, for twelve azimuthal planes of rotation in

ϕ, i.e., a full 4π steradians. Frequency-dependent measurements were subsequently performed at field orientations parallel to the deduced magnetic symmetry axes. All simulations were performed using the program EasySpin.[31]

III. RESULTS

Structural Characterization: Single-crystal x-ray diffraction studies of **1** and **2** show that the molecules crystallize in an orthorhombic unit cell.[32] The crystals were obtained via slow vapor diffusion of dichloromethane into a solution of 1,1,2,2-tetrachloroethane containing the complex.[27] Interestingly, concentrations above 4.5 mM yield crystals in the $P2_12_12_1$ space group, while lower concentrations lead to the *Pnma* space group. In the $P2_12_12_1$ space group, a total of four distinct (differently oriented) molecules are contained within the unit cell while, in the *Pnma* space group, only two independent molecules are found. Due to these observations, we focus here exclusively on the complexes crystallizing in the *Pnma* space group because they are expected to exhibit less complex spectroscopic behavior.

We describe only the structural characteristics of **1**, as it exhibits the most interesting spectroscopic properties. Single-crystal x-ray studies reveal only half of the molecule residing in the asymmetric unit, with two differently oriented molecules and a total of four molecules within the unit cell [Fig. 1(c)]. The two spatially different molecules are related by a rotation about the crystallographic *b*-axis of ~70º. Locally, the Tb^{III} ion resides in a very symmetric environment. The eight isoindole nitrogens of the Pc_2 ligands impose a square antiprismatic coordination geometry on the Tb^{III} ion, with the two Pc ligands arranged above and below in a near perfect staggered configuration. The average distance to the eight coordinating nitrogens is 2.4186(2) Å, while the mean distance to the planes of the Pc ligands is 1.4064(1) Å. Note that the distances observed here for the neutral $[TbPc_2]^0$ (**1**) are slightly shorter than those reported for the negatively-charged analog, $TBA^+[TbPc_2]^-$,[33] where the $\langle Tb\cdots N\rangle$ and $\langle Tb\cdots Pc\rangle$ distances are 2.8245(3) and 1.4122(3) Å, respectively. The average twist angle between the two Pc moieties is 45º [Fig. 1(b)], compared to 44.1º for the $TBA^+[TbPc_2]^-$ analog. Therefore, the Tb^{III} ion of **1** experiences a near ideal local D_{4d} crystal field symmetry.

Spectroscopy: EPR spectra collected on powder samples of **1** and **2**, at a frequency of 104.8 GHz and a temperature of 5 K, are shown in Fig. 2. The $[YPc_2]^0$ complex (**2**) displays a sharp signal at

~3.75 T (peak-to-peak linewidth ~5 mT), corresponding to an isotropic Landé *g*-factor of 2.003(1) that can be ascribed to the spin-½ radical; the 1st derivative lineshape results from the lock-in detection of the field modulated signal, *dI*/*dB*, where *I* represents the absorption intensity. By contrast, the EPR spectrum of $[TbPc_2]^0$ (**1**) shows a significantly broader spectrum, with two prominent features spanning all the way from the strong 1st derivative signal at 2.93 T (peak-to-peak linewidth ~37 mT) to the weaker asymmetric dip at the isotropic $g = 2.00$ position (~3.75 T). Such a powder spectrum is typical for a species experiencing an axial magnetic anisotropy, with the two features corresponding to the parallel and perpendicular components. It is worth noting that the EPR spectrum of the charged $TBA^+[TbPc_2]^-$ derivative, for which the radical is absent, does not show any visible EPR transition. This confirms a strong axiality and negligible mixing within the ground $m_J = \pm 6$ substates of the Tb^{III} ion, such that the transition between them is strongly forbidden. Consequently, the entire spectrum recorded for the $[TbPc_2]^0$ complex is ascribable to the radical. In turn, the anisotropic nature of this spectrum provides the first indication that the radical is coupled to the Tb^{III} ion, because an isolated radical would otherwise give the same narrow spectrum as the $[YPc_2]^0$ complex.

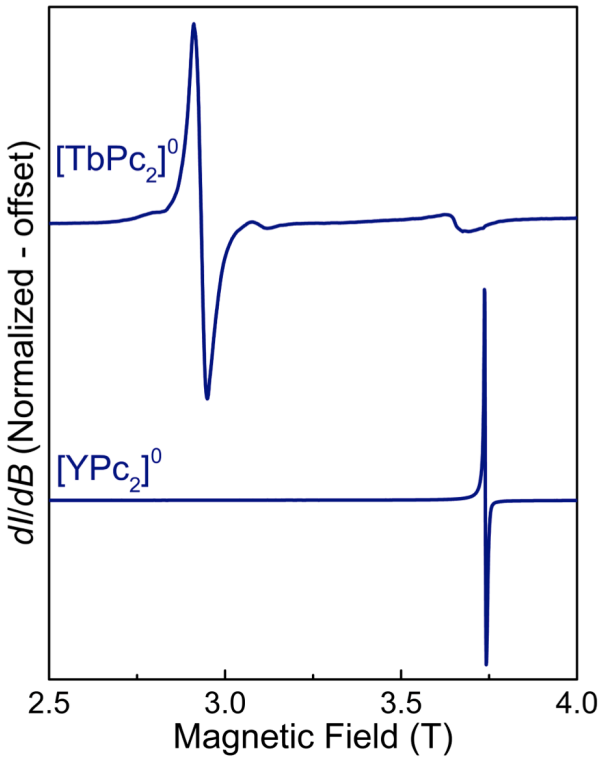

Fig. 2. Powder EPR spectra collected on samples of **1** and **2** at a frequency of 104.8 GHz and a temperature of 5 K; the data were recorded in derivative mode, *dI*/*dB* (*I* = absorption intensity).

Single-crystal EPR measurements were subsequently carried out on **1** in order to study the effect of the lanthanide ion on the radical in more detail. Angle-dependent spectra collected at 65.5 GHz and 2 K for a full 180° rotation of θ (with $\phi = 120°$) are shown in Fig. 3. Two sharp angle-dependent resonances of comparable linewidth to those observed for the pure radical (Fig. 2) are seen at essentially all angles (except at $\theta = 90°$, where they merge to a single asymmetric resonance). This, together with the field dependence (*vide infra*), which ascribes *g*-factors of ~2.00 to both resonances, corroborates their assignment to the spin-½ radicals. The fact that the separation of the parallel and perpendicular components of the 104.8 GHz powder spectrum (~0.82 T, see Fig. 2) is comparable to the range of the 65.5 GHz single-crystal data in Fig. 3 suggests a field-independent anisotropic interaction, likely involving a coupling of the radical to the terbium ion, as the spectrum would otherwise be isotropic. Meanwhile, the fact that two EPR transitions are observed with distinct angle-dependences can be attributed to the existence of two differently oriented molecules within the unit cell of compound **1** [Fig. 1(c)]. By following the evolution of the resonance positions with angle, it is straightforward to assign each one to a given molecular orientation, as seen in Fig. 3.

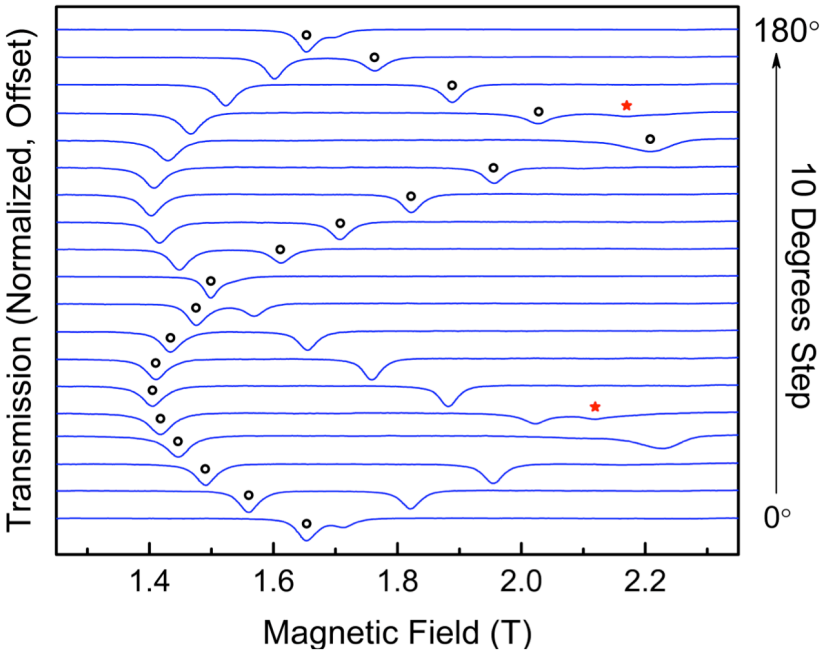

Fig. 3. Angle-dependent EPR spectra for a single crystal of **1** for a full 180° rotation of θ (with $\phi = 120°$), collected at a frequency of 65.5 GHz and temperature of 2 K; the dips in transmission correspond to the resonances. The green circles denote resonances for one of the two molecular orientations: note the smooth variation with angle from the cusp-like maximum (at ~2.2 T), through a broad minimum (at ~1.4 T), with an overall 180° periodicity. An additional weak resonance is observed at two of the angles (marked with *), which we explain in Section IV.

Additional data sets under the same conditions as those displayed in Fig. 3 were collected for multiple azimuthal planes of rotation. Fig. 4 displays 3D color maps representing these angle-dependences mapped onto a complete sphere. Because there is more than one resonance for each field orientation, the data are presented in several ways, emphasizing different aspects of the magnetic anisotropy of **1**: (a) plots the position of the lowest resonance field, highlighting the easy directions (dark blue); (b) plots the position of the highest resonance field, accentuating the hard directions (red); and (c) plots the resonance position for only one of the two molecular orientations. The color maps clearly indicate an easy-axis anisotropy for both molecular orientations, i.e., the hard directions are confined to planes, with easy directions along two axes that are orthogonal to the hard planes. Moreover, the hard-planes/easy-axes are tilted ~70° with respect to each other, in excellent agreement with the orientations of the two $[TbPc_2]^0$ molecules determined from X-ray diffraction measurements [Fig. 1(c)].

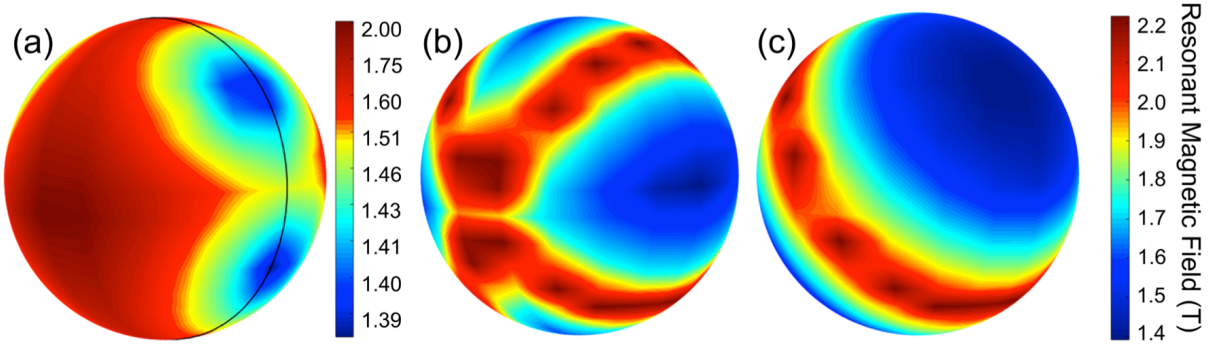

Fig 4. 3D color maps of the positions of the lowest (a) and highest (b) field 65.5 GHz EPR positions, highlighting the easy (blue) and hard (red) magnetization directions of the Tb^{III} ion, respectively; the black line in (a) marks the $\phi = 120^o$ plane of rotation, which intersects the easy axes of the two differently oriented molecules (see Fig. 3). (c) Resonance position for one of the two molecular orientations, clearly indicating an easy-axis anisotropy. The two hard-planes and easy-axes are tilted ~70° with respect to each other, in excellent agreement with the orientations of the two $[TbPc_2]^0$ molecules (see Fig. 1).

From the above measurements, it is straightforward to locate the magnetic symmetry axes/planes for each molecular orientation. In fact, the crystal was mounted within the resonator such that the $\phi = 120^o$ azimuthal plane approximately intersects the easy-axes (and hard-planes) of both orientations [see Fig. 4(a)]; note that this corresponds to the situation in Fig. 3. For this plane of rotation, one can therefore define polar angles, ψ_1 and ψ_2, that represent the alignment of the applied magnetic field with respect to the easy-axes of the two molecular orientations. Such a transformation from the laboratory frame (θ, ϕ) to local coordinates (ψ_i) is illustrated in Fig. 5, which displays the ψ-dependence of the resonance positions for one of the molecular

orientations in Fig. 3: the easy- ($\psi = 0$) and hard- ($\psi = \pm 90^{o}$) directions are noted in the figure, and simulated angle-dependences (*vide infra*) are superimposed on the data.

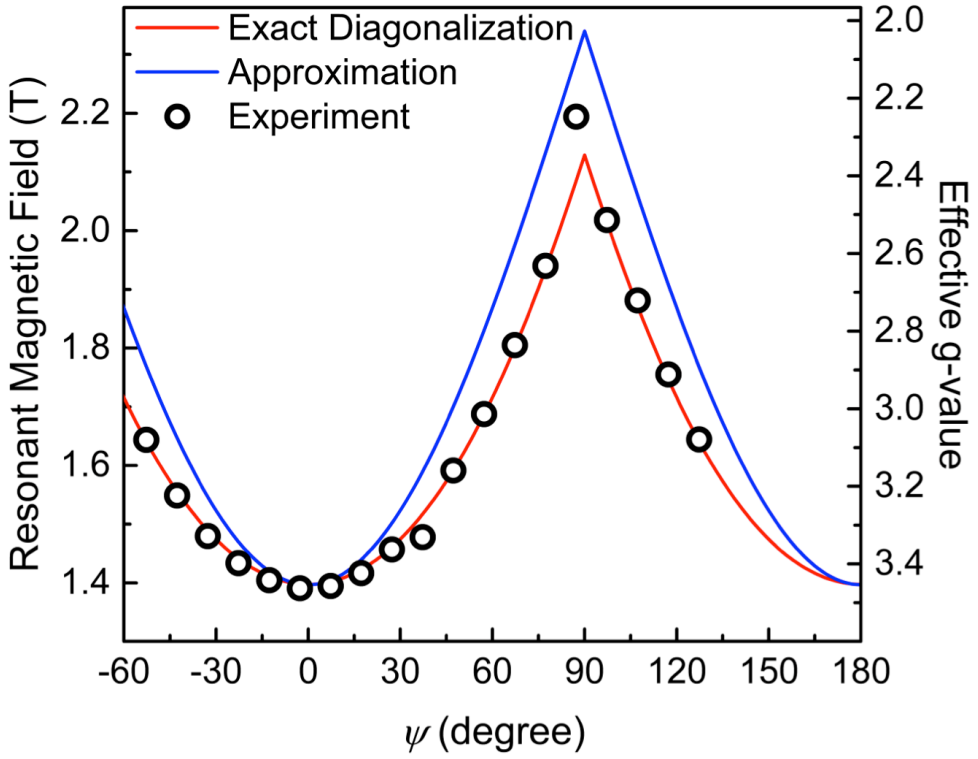

Fig. 5. Plot of the resonance positions in Fig. 3 [see also Fig. 4(a)], for one of the two molecular orientations; the polar coordinate has been transformed ($\theta \rightarrow \psi$) to a local frame, where $\psi = 0$ represents field parallel to the easy axis of the molecule. The solid curves represent two different simulations described in Section IV, one exact and the other approximate.

Figure 6 plots the frequency dependence of resonance positions for the easy- ($\psi = 0$) and hard- ($\psi = 90^{o}$) directions of $[TbPc_2]^0$ (**1**). As noted above, the magnitude of the anisotropy, as measured by the separation of the $\psi = 0$ and 90^{o} resonances, is field-independent. Moreover, agreement between the single-crystal and powder data is good over the entire range investigated. Importantly, the ~26 GHz zero-field intercept/gap in the spectrum cannot be explained in terms of non-interacting spin-½ radicals; Kramers' theorem forbids such a gap.[34] Superimposed on the data in Fig. 6 are simulations that assume a ferromagnetic coupling between the radical and the Tb^{III} ion on each molecule; details concerning these simulations, which assume an isotropic *g*-factor of ~2.00 and just a single interaction parameter, are given in the following section . As can be seen, agreement between the experiment and simulation is excellent.

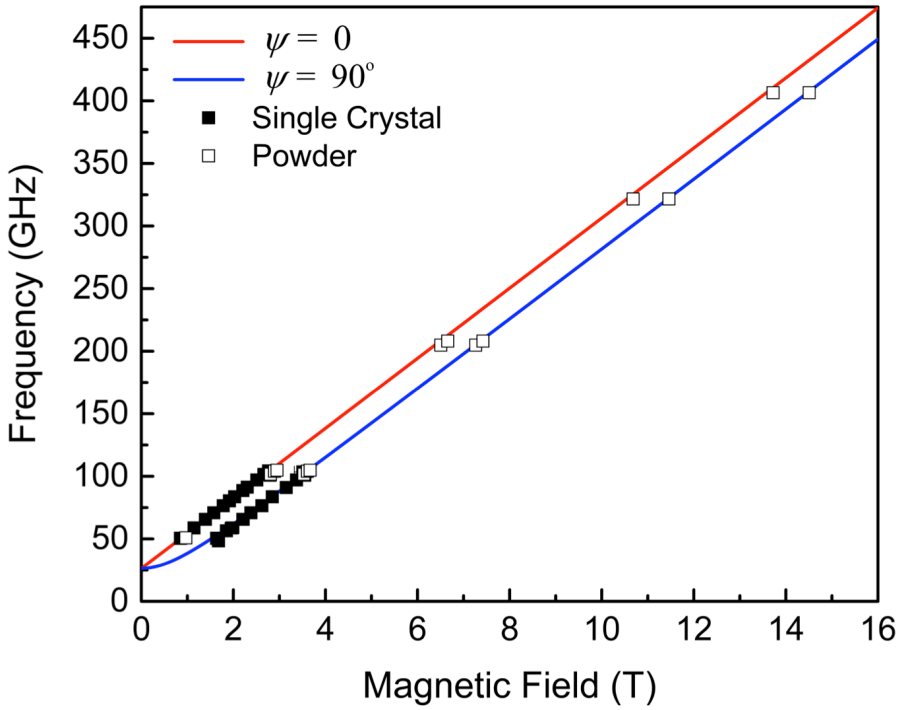

Fig. 6. Frequency versus magnetic field plot of the combined single-crystal (at T = 2 K) and powder (at T = 5 K) EPR data for **1**, with the field parallel ($\psi = 0$) and perpendicular ($\psi = 90$)° to the easy axis of one of the molecular orientations; uncertainties in the determination of the resonance positions lie within the data points. The solid lines represent simulations described in Section IV.

IV. DISCUSSION

The preceding experiments provide clear evidence that the EPR signals seen for compounds **1** and **2** can be attributed, to zeroth-order, to the unpaired spin-½ on the Pc_2 radical. We now consider the source of considerable anisotropy of the radical signal in **1**. While rare, EPR spectra exhibiting similar degrees of anisotropy have been reported for crystals of magnetically ordered organic radical ferromagnets.[35,36] However, a smooth first-order angle-dependence (~$\sin^2\psi$) is observed in these cases, as opposed to the cusp-like behavior observed at $\psi = 90$° in **1**. Moreover, the isotropic signal observed for **2** would also seem to rule out the possibility that long range ordering of the radicals is responsible for the anisotropy in **1**. Hence, coupling to the highly anisotropic Tb^{III} ion represents the obvious starting point for an analysis of the results.

We thus consider the simplest possible effective spin Hamiltonian of Eq. (1) that includes an isotropic (scalar) coupling between the radical and Ln moments, while absorbing all of the anisotropy into the zero-field-splitting (ZFS) Hamiltonian, $\hat{H}_{\mathrm{ZFS}}^{\mathrm{Tb}}$, of the terbium ion:

$$\hat{H}^{\mathrm{eff}} = \hat{H}_{\mathrm{ZFS}}^{\mathrm{Tb}} + J_{\mathrm{ex}}\hat{S}^{\mathrm{rad}} \cdot \hat{J}^{\mathrm{Tb}} + \hat{H}_{\mathrm{Z}}^{\mathrm{Tb}} + \hat{H}_{\mathrm{Z}}^{\mathrm{rad}}. \qquad (1)$$

Here, $\hat{S}^{\mathrm{rad}}$ and $\hat{J}^{\mathrm{Tb}}$ respectively represent angular momentum operators associated with the radical (spin) and the lanthanide (spin-orbital), while J_{ex} parameterizes the scalar coupling between them. Meanwhile, we assume isotropic Zeeman interactions, $\widehat{H}_{\mathrm{Z}}^{\mathrm{Tb}}$ $\left(= g_J \mu_B \vec{B}_0 \cdot \hat{J}^{\mathrm{Tb}}\right)$ and $\widehat{H}_{\mathrm{Z}}^{\mathrm{rad}}$ $\left(= g_e \mu_B \vec{B}_0 \cdot \hat{S}^{\mathrm{rad}}\right)$, with g_e (= 2.00) and g_J (= 3/2 for Tb^{III}) representing the Landé factors, and $\vec{B}_0$ the applied magnetic field.

The anisotropic ZFS interaction of the Tb^{III} ion can be expressed in terms of extended Stevens' operators:[37]

$$\widehat{H}_{\mathrm{ZFS}}^{\mathrm{Tb}} = \sum_{k=2,4,6} \sum_{q=-k}^{k} B_k^q \, \widehat{O}_k^q \qquad (2)$$

The $\hat{O}_k^q$ terms are comprised of angular momentum operators of rank k, which are then parameterized by their accompanying B_k^q coefficients. The off-diagonal ($q \neq 0$) terms can be neglected for the purposes of this analysis, as they are known to influence the magnetic behavior of the Tb ion only at very low applied magnetic fields ($B_0 < 0.04$ T).[25] This leaves only the cylindrically symmetric terms, $B_k^0 \hat{O}_k^0$ ($k = 2,\ 4,\ 6$), containing only even powers of the z-component angular momentum operator, $\hat{J}_z^k$, where we have dropped the 'Tb' superscript here for compactness. In principle, the B_k^0 coefficients are known from thermodynamic measurements.[24,25] However, we find that the results of the simulations are completely insensitive to these parameters provided they are chosen so that the $m_J = \pm 6$ substates lie lowest in energy and are well separated from the first excited state, as is known to be the case experimentally. For these purposes, one can simplify the analysis greatly by retaining only the leading term $B_2^0 \hat{O}_2^0 = \left\{3\hat{J}_z^2 - \hat{J}\left(\hat{J}+1\right)\right\}$, so long as the B_2^0 parameter is chosen to be negative and sufficiently large so that the Tb^{III} ZFS interaction dwarfs the remaining interactions in Eq. (1), i.e., the EPR measurements do not constrain this parameter (or any of the Tb^{III} ZFS parameters).[38]

The approach outlined above leaves J_{ex}, the scalar coupling, as the only free parameter in the model. The simulations in Figs. 5 and 6 assume a ferromagnetic interaction, $J_{\mathrm{ex}} = -0.147$ cm^{-1}. It is now relatively straightforward to understand the experimental observations within the context of this relatively simple model. In zero-field, the radical is coupled only to the Tb^{III} ion, with doubly degenerate eigenstates $\left|+6, +\tfrac{1}{2}\right\rangle$, $\left|-6, -\tfrac{1}{2}\right\rangle$, and $\left|+6, -\tfrac{1}{2}\right\rangle$, $\left|-6, +\tfrac{1}{2}\right\rangle$, employing here an

$|m_J, m_S\rangle$ representation. The energy separation between these states, $\Delta_0 = |6J_{ex}| = 0.88$ cm^{-1} or 26.4 GHz, corresponding to the zero-field gap in the EPR spectrum (see Fig. 6); as can be seen, the transitions $|+6, +\frac{1}{2}\rangle$ to $|+6, -\frac{1}{2}\rangle$ and $|-6, -\frac{1}{2}\rangle$ to $|-6, +\frac{1}{2}\rangle$, involve a simple spin-flip of the radical under an exchange bias field due to the Tb^{III} ion, i.e., the gap corresponds to the energy difference between the ferro- (F) and antiferromagnetic (A) configurations (meaning up/up and up/down, not to be confused here with long-range ordered states).

We next consider the field dependence of the EPR spectrum. Because of the strong crystal-field anisotropy of the Tb^{III} ion, it may be treated as an Ising-like moment, i.e., $\langle \hat{J}_x^{Tb} \rangle = \langle \hat{J}_y^{Tb} \rangle = 0$. Consequently, from a semi-classical point-of-view, the Tb^{III} moment is constrained along $\pm z$, the C_4 symmetry axis of the molecule (or $\psi = 0^o$). Meanwhile, in the intermediate field regime, the radical spin follows B_0; here, 'intermediate' implies that the radical Zeeman interaction, $\hat{H}_Z^{rad}$, is strong enough to overcome the scalar coupling (i.e., $g_e \mu_B B_0 > \Delta_0$), but that the field is not yet so strong that it can compete with $\hat{H}_{ZFS}^{Tb}$. The scalar interaction energy then takes the form:

$$J_{ex} \hat{S}^{rad} \cdot \hat{J}^{Tb} \approx \pm J_{ex} \left| \frac{1}{2} \frac{\vec{B}_0}{B_0} \cdot 6\hat{z} \right| = \pm 3 |J_{ex} \cos\psi|, \qquad (3)$$

where the ± signs denotes the F (–) and A (+) cases. Likewise, in this same intermediate field regime, the radical and Tb^{III} Zeeman interactions may be written:

$$\hat{H}_Z^{Tb} \approx \pm \frac{3}{2} \mu_B \left| \vec{B}_0 \cdot 6\hat{z} \right| = \pm 9 \mu_B B_0 |\cos\psi|$$

$$\hat{H}_Z^{rad} \approx \pm \mu_B B_0. \qquad (4)$$

The absolute value of the cosine recognizes the time-reversal invariance of the leading axial interaction, $\hat{H}_{ZFS}^{Tb}$, which means that the physics is the same regardless of whether the field is applied above or below the molecular hard-plane. One can then write down expressions for the four energy eigenvalues, referenced to the uncoupled zero-field ground state energy:

$$\epsilon_{0\pm} \approx -|3J_{ex} \cos\psi| \pm 9\mu_B B_0 |\cos\psi| \pm \mu_B B_0;$$

$$\epsilon_{1\mp} \approx +|3J_{ex} \cos\psi| \pm 9\mu_B B_0 |\cos\psi| \mp \mu_B B_0, \qquad (5)$$

where ε_0 and ε_1 correspond to the F and A cases, respectively (see Fig. 7); the inverted $\mp$ in the 2nd expression reflects the A coupling, i.e., the radical is 'down' when the Tb^{III} is 'up'. Radical

EPR transitions involve a change in the sign of the last terms in Eq. (5), but no change in the 2nd terms (the Tb^{III} Zeeman energy). The ground state transition, ϵ_{0-} to ϵ_{1+}, thus involves an energy

$$\Delta\epsilon_0 \approx |6J_{\rm ex}\cos\psi| + 2\mu_B B_0. \qquad (6)$$

Although Eqs. (3) to (6) are approximate, they become exact for $\psi = 0^{\rm o}$, because the Hamiltonian of Eq. (1) is diagonal in this limit. Therefore, $\Delta\epsilon_0 = \Delta_0 + 2\mu_B B_0$ for this orientation, i.e., the unperturbed transition energy ($g_e\mu_B B_0$, with $g_e = 2.00$) for the radical is offset vertically by the zero-field gap, $\Delta_0 = |6J_{\rm ex}|$, exactly as observed in Fig. 6. Meanwhile, for $\psi = 90^{\rm o}$, the scalar coupling and Tb^{III} Zeeman interactions are identically zero in the intermediate field regime (because $\hat{S}^{\rm rad}\cdot\hat{J}^{\rm Tb} = \vec{B}_0\cdot\hat{J}^{\rm Tb} = 0$), resulting in an EPR spectrum that is indistinguishable from that of an isolated radical, i.e., a $g_e = 2.00$ resonance with no zero-field offset, again in reasonable agreement with experiment (Fig. 6).

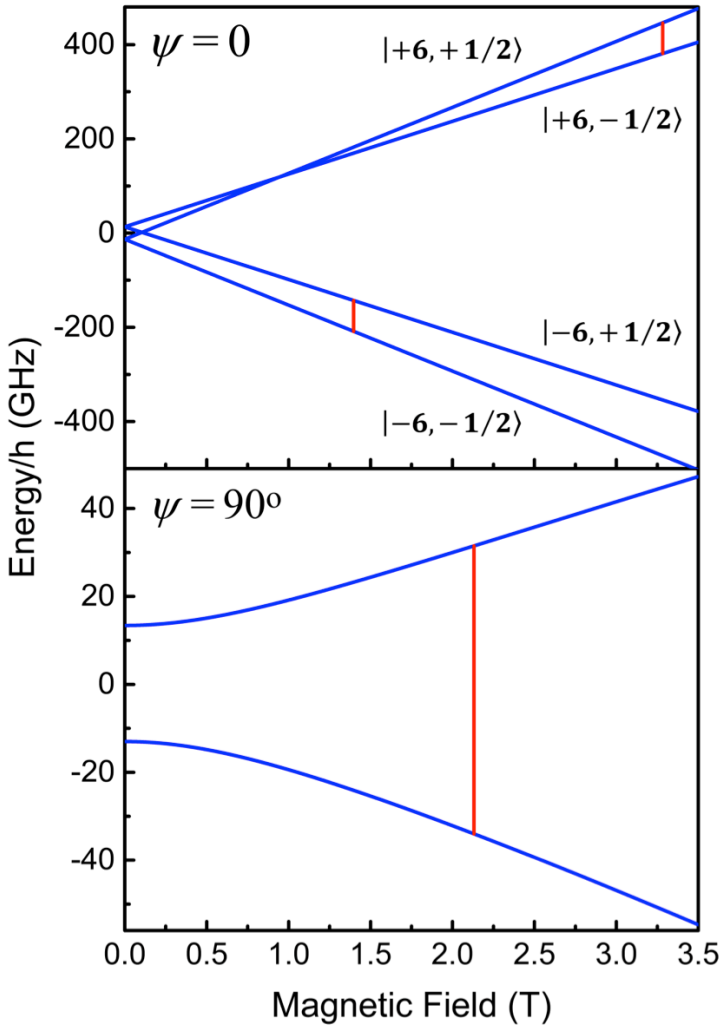

Fig. 7. Exact solutions to Eq. (1) with the field applied parallel (a) and perpendicular (b) to the easy axis of the $[TbPc_2]^0$ molecule; note that each of the solutions in (b) is doubly degenerate. The red lines denote allowed EPR transitions at 65.5 GHz, corresponding to a spin-flip of the radical.

The overall effect of the scalar coupling is to shift the ground state EPR positions by an amount,

$$\Delta B_0 \approx -\left|\frac{3J_{\mathrm{ex}}\cos\psi}{\mu_B}\right|, \tag{7}$$

below the isotropic $g = 2.00$ position (~2.34 T at 65.5 GHz), where $|3J_{\mathrm{ex}}/\mu_B| \approx 0.94$ T. Here, one sees the reason for the cusp-like turning point of the resonance position at $\psi = 90^{\mathrm{o}}$ and the broad minimum at $\psi = 0^{\mathrm{o}}$ (Fig. 5). The experimental downshift shift of 0.94 T to 1.4 T at $\psi = 0^{\mathrm{o}}$ is in excellent agreement with experiment. However, the angle dependent data presented in Fig. 5 were obtained slightly below the 'intermediate' field regime, so that the approximation does not work as well when the field rotates away from $\psi = 0^{\mathrm{o}}$. The scalar interaction dominates at low fields, meaning that there is a residual coupling to the Tb^{III} ion even at $\psi = 90^{\mathrm{o}}$, thus explaining why the resonance occurs slightly below the $g = 2.00$ position. Indeed, this is also the reason why Eq. (7) does not account quantitatively for the experimental results in Fig. 5 quite as well as the simulations involving exact diagonalization of Eq. (1); comparisons between the exact and approximate expressions at much higher fields do give near perfect agreement.

For the magnetic fields (>1 T) and temperatures (~2 K) at which the experiments were carried out, only the $|-6,-\frac{1}{2}\rangle$ (at ϵ_{0-}) and $|-6,+\frac{1}{2}\rangle$ (at ϵ_{1+}) states are significantly populated when the applied field has an appreciable component along z; this is because of the strong Zeeman interaction associated with the Tb^{III} ion ($\pm 9\mu_B B_0|\cos\psi|$). Hence, only the ground state EPR transition is observed for most field orientations. However, this is not necessarily the case when ψ is close to 90°. In fact, the $\epsilon_{0\pm}$ and $\epsilon_{1\mp}$ states are quasi-degenerate at exactly $\psi = 90^{\mathrm{o}}$, because the radical EPR transition is insensitive to the state of the Tb^{III} ion, which lives in a non-magnetic superposition of the $m_J = \pm 6$ states (with a miniscule tunneling gap on the order of kHz).[25] Thus, one may think of two (quasi-) degenerate radical EPR transitions, one for each of the Tb^{III} degrees of freedom. Meanwhile, slightly away from $\psi = 90^{\mathrm{o}}$, this degeneracy is lifted because of the weak longitudinal (//z) field component, yet both transitions may be expected to possess detectable Boltzmann weights, thereby explaining the observation of an additional peak

at some orientations close to $\psi = 90^{o}$ in Fig. 3 (indicated by *). However, the intensity of the higher-lying transition will rapidly lose weight as the field rotates away from $\psi = 90^{o}$.

It is natural to question the validity of such a simple model [Eq. (1)]. In particular, why assume a scalar coupling? Exchange involving spin-orbital moments only couples the spin part of the wavefunction and, for instance in Ref. [12], we have expressed this Heisenberg interaction as $J_{\mathrm{ex}}\hat{S}^{\mathrm{rad}} \cdot \hat{S}^{\mathrm{Tb}}$. However, our choice here does not alter the underlying physics, because $\vec{L}$ is strongly coupled to $\vec{S}$, and the net effect would simply be a renormalization of the coupling parameter, J_{ex}, doubling its value in the case of Tb^{III}. Similarly, why not consider an anisotropic coupling, such as an Ising or dipolar interaction? The Ising character is already built into the model via the ZFS interaction associated with the Tb^{III} ion. An anisotropic coupling ($\overleftrightarrow{J}_{\mathrm{ex}}$ is now a tensor) would simply add superfluous parameters. We note that recent CASSCF (Complete Active Space Self-Consistent Field) ab initio calculations[12,39] on $[TbPc_2]^0$ using a minimal active space of 4*f* orbitals and the π-ligand singly occupied molecular orbital (π-SOMO), also including spin-orbit coupling non-perturbatively, fully support our current assumption that the radical-4*f* exchange coupling is: (i) much smaller than the gap between ground and first excited crystal field substates; and (ii) well described by an isotropic exchange Hamiltonian.

Another potential source of anisotropic coupling that should be considered is the purely through-space dipolar interaction between the Tb^{III} ion and the spin density on the radical, which can in principle be calculated precisely via ab-initio methods. However, one can also get a good sense for the magnitude of this interaction by assuming that the radical spin density is localized on the C and N atoms of the ligand, and then performing simple point-dipole calculations. Published density functional theory (DFT) results suggest that most of the spin density resides on the 16 inner C atoms (on average 0.05 μ_B/C), which are located at an average distance of 3.33 Å from the Tb^{III} ion.[17] Meanwhile, the remainder of the density resides on the 48 C atoms of the outer rings (0.005 μ_B/C), with a small negative polarization on the 16 coordinating N atoms (about –0.01 μ_B/N). Interestingly, based on a point dipole approximation, we find the coupling to be antiferromagnetic for nearly all of these sites. The closest 8 N atoms sit at an average angle of 54.55^{o} from the Tb ion, as measured from the C_4 axis of the molecule. This is fractionally below the magic angle of $\psi_m = 54.7^{o}$ [$3\cos^2\psi_m - 1 = 0$], meaning that the contribution of these sites to the dipolar interaction is near negligible because of the axial symmetry of the molecule.

Moreover, because the polarization is negative at these sites, their contribution to the coupling will be antiferromagnetic. The remaining atoms all sit at angles beyond ψ_m. Therefore, the remaining 8 N atoms provide the only ferromagnetic coupling. However, this contribution is overwhelmed by the carbon atoms, which all couple antiferromagnetically to the Tb^{III} ion. A weighted sum of point-dipolar contributions gives an estimate for the ZFS of $\Delta_0 \approx 1.3$ GHz, corresponding to a $J_{ex} = +7.2 \times 10^{-3}$ cm^{-1}. Thus, not only is the sign incorrect, the magnitude of the coupling is more than an order of magnitude too small. Therefore, the main contribution to the coupling has to involve exchange, and Eq. (1) is expected to capture the essential physics.

There have been a limited number of previous (and conflicting) experimental and theoretical attempts to evaluate the radical-lanthanide exchange interaction in bis-phthalocyaninato-type Ln complexes. The earliest study on $[LnPc_2]^0$ suggested a strong antiferromagnetic coupling (when Ln = Gd, Tb, Ho) on the basis of relatively high-temperature magnetic susceptibility measurements.[18,19] More recently, both ferro- and antiferromagnetic interactions have been deduced from single-molecule transistor experiments,[15,17] although a large anisotropic exchange term (amounting to 60% of the isotropic component) was introduced in Ref. [17] in order to explain some features of the observed Kondo resonance. Meanwhile, recent NMR/DFT studies on a very similar $[TbPc_2]^0$ complex to the one studied here have suggested ferromagnetic coupling due to the orthogonality between the broken-symmetry ligand-centered π-SOMO and the seven 4*f* magnetic orbitals with opposite spin polarization.[40] We note, however, that the energies of the high- and low-spin states of $[GdPc_2]^0$ were not reported in Ref. [40], so it is difficult to assess whether other exchange mechanisms (e.g., spin-polarization) could stabilize an antiferromagnetic ground state, despite the orthogonality between magnetic orbitals. Another quite recent DFT calculation shows that the exchange coupling between the *f*-electrons and the radical is mediated by *d*-electrons of the Tb^{III} ion that significantly overlap the N and C orbitals of the Pc ligands and, due to large spin-polarization effects, lead to antiferromagnetic coupling.[11] Meanwhile, combined XMCD, CASSCF/RASSI-SO and DFT studies of $[TbPc_2]^0$ grafted onto surfaces point to ferromagnetic coupling,[12] although the results depend on the details of the modeling and are sensitive to molecule configuration.

The present EPR experiments undoubtedly demonstrate a ferromagnetic Tb-radical exchange interaction in the bulk $[TbPc_2]^0$ derivative crystallized in the *Pnma* space group. One may actually expect such coupling on the basis of relatively simple molecular point group symmetry

considerations.[39] It turns out that, for exact molecular D_{4d} symmetry, the π-SOMO (ϕ_π) on the Pc_2 ligand system spans a $\Gamma_\pi = a_2$ irreducible representation of D_{4d}, while the irreducible representations spanned by the 4*f* orbitals of the central Tb^{III} ion are $\Gamma_{4f} = b_2 + e_1 + e_2 + e_3$.[39] Therefore, the kinetic contribution to the exchange, proportional to the matrix element of a totally symmetric Hamiltonian, *h*, inducing virtual transitions between the π-SOMO and the Tb 4*f* atomic orbitals, is clearly zero by symmetry, i.e. $\langle \phi_\pi | h | 4f \rangle = 0$, since $\Gamma_\pi \times \Gamma_{4f}$ does not include the totally symmetric irreducible representation. It is this contribution that favors antiferromagnetic coupling.[35] Therefore, its absence leaves only potential exchange within the restricted excitation space of the π-SOMO and seven 4*f* orbitals. This interaction is given by the exchange integral, which is always ferromagnetic and necessarily isotropic. Consideration of extended excitation spaces may introduce additional (likely weaker) terms, both isotropic and anisotropic, and of either sign.[35,39] However, the simple symmetry arguments presented here seem to confirm the ferromagnetic coupling that is found experimentally.

Finally, Branzoli et al. reported an antiferromagnetic inter-molecular exchange interaction between $[YPc_2]^0$ radicals (here, Y is non magnetic) from magnetization, ^1H NMR paramagnetic shifts and NMR T_1 measurements.[41] Meanwhile, specific heat measurements on $LnPc_2$ (Ln = Y, Tb) also evidence the presence of extended spin excitations at low temperature.[42] Effects of such inter-molecular interactions are not evident in the single-crystal EPR measurements presented here; in particular, the observation of independent (non-interacting) signals for the two molecular orientations would seem to rule this out. However, weak satellite peaks observed in the powder measurements (~0.15 T above and below the strong low-field resonance in Fig. 1), at the lowest temperatures, may provide evidence for intermolecular interactions in the $P2_12_12_1$ structure (γ phase). These satellite peaks have no counterpart in the single-crystal EPR measurements. However, Xray structure studies of the powder sample employed in this study suggest a small contamination with the $P2_12_12_1$ phase. Future work aims to address the issue of intermolecular exchange interactions in $Ln(Pc)_2$ crystals in more detail.

V. CONCLUSIONS

We present detailed high-field, high-frequency EPR measurements on a powder and a single-crystal sample of a previously unreported structural phase (*Pnma* space group) of the neutral terbium bis-phthtalocyaninato metalorganic complex, $[TbPc_2]^0$. An anisotropic EPR spectrum is

observed, which is attributed to the $s = ½$ radical delocalized over the Pc_2 ligand. The magnetic anisotropy results from a weak coupling of the radical to the Ising-like spin-orbital moment of the Tb^{III} ion. Angle-dependent EPR studies reveal two differently oriented, magnetically independent molecules, in agreement with Xray structural studies. Analyses of the results unambiguously demonstrate that the radical-Tb^{III} coupling is due to a ferromagnetic exchange interaction. The essential physics is captured via an effective spin Hamiltonian in which the exchange is assumed to be isotropic ($J_{ex} = -0.147$ cm^{-1}), while the magnetic anisotropy is folded entirely into the single-ion properties of the Tb^{III} ion. This model is rationalized on the basis of the simple symmetry considerations that dictate an orthogonality of the Tb 4*f* orbitals and the π-SOMO associated with the Pc_2 ligand, thereby suppressing virtual hopping transitions that mediate antiferromagnetic exchange interactions.

VII. SUPPLEMENTAL MATERIALS

The crystallographic data for the structures have been included in CIF format in the online Supplemental Material. These have also been deposited with the Cambridge Crystallographic Data Centre, structures CCDC 1569653 (**1**) and CCDC 1569654 (**2**).

VII. ACKNOWLEDGEMENTS

We acknowledge financial support from the US National Science Foundation (DMR-1610226), the Air Force Office of Scientific Research (Asian Office of Research and Development, contract FA2386-17-1-4040), the Italian Ministry of Education and Research (MIUR) though the PRIN project 2015HYFSRT, the DFG-TR 88 "3Met", and ANR-13-BS10-0001-03 MolQuSpin. AS and MA acknowledge financial support from the Australian Research Council, Discovery Grant ID: DP15010325. A portion of this work was performed at the US National High Magnetic Field Laboratory, which is supported by the National Science Foundation (DMR-1157490) and the State of Florida. We also acknowledge the Karlsruhe Nano Micro Facility (KNMF, www.kit.edu/knmf) for providing access to instruments at their laboratories.

VIII. REFERENCES CITED

* To whom correspondence should be sent: marco.affronte@unimore.it, shill@magnet.fsu.edu.

[1] K.L.M. Harriman, A.A. Leitch, S.A. Stoian, F. Habib, J.L. Kneebone, S.I. Gorelsky, I. Korobkov, S. Desgreniers, M.L. Neidig, S. Hill, M. Murugesu, and J.L. Brusso, Ambivalent binding between a radical-based pincer ligand and iron, Dalton Trans. **44**, 10516 (2015).

[2] E.C. Constable, 2,2′:6′,2″-Terpyridines: From chemical obscurity to common supramolecular motifs, Chem. Soc. Rev. **36**, 246 (2007).

[3] E.A. Medlycott and G.S. Hanan, Designing tridentate ligands for ruthenium(II) complexes with prolonged room temperature luminescence lifetimes, Chem. Soc. Rev. **34**, 133 (2005).

[4] R. Shunmugam, G.J. Gabriel, K.A. Aamer, and G.N. Tew, Metal–Ligand-Containing Polymers: Terpyridine as the Supramolecular Unit, Macromol. Rapid Commun. **31**, 784 (2010).

[5] C. Benelli, A. Caneschi, D. Gatteschi, and R. Sessoli, Magnetic interactions and magnetic ordering in rare earth metal nitronyl nitroxide chains, Inorg. Chem. **32**, 4797 (1993).

[6] L. Bogani, C. Sangregorio, R. Sessoli, and D. Gatteschi, Molecular Engineering for Single-Chain-Magnet Behavior in a One-Dimensional Dysprosium–Nitronyl Nitroxide Compound, Angew. Chemie - Int. Ed. **44**, 5817 (2005).

[7] K. Bernot, L. Bogani, A. Caneschi, D. Gatteschi, and R. Sessoli, A Family of Rare-Earth-Based Single Chain Magnets: Playing with Anisotropy, J. Am. Chem. Soc. **128**, 7947 (2006).

[8] W. J. Evans, D. S. Lee, D. B. Rego, J. M. Perotti, S. A. Kozimor, E. K. Moore, J. W. Ziller, Expanding Dinitrogen Reduction Chemistry to Trivalent Lanthanides via the LnZ_3/Alkali Metal Reduction System: Evaluation of the Generality of Forming $Ln_2(\mu\text{-}\eta^2\text{:}\eta^2\text{-}N_2)$ Complexes via LnZ_3/K, J. Am. Chem. Soc. **126**, 14574 (2004).

[9] J J.D. Rinehart, M. Fang, W.J. Evans, and J.R. Long, A N_2^{3-} Radical-Bridged Terbium Complex Exhibiting Magnetic Hysteresis at 14 K, J. Am. Chem. Soc. **133**, 14236 (2011).

[10] J.D. Rinehart, M. Fang, W.J. Evans, and J.R. Long, Strong exchange and magnetic blocking in N_2^{3-}-radical-bridged lanthanide complexes, Nat. Chem. **3**, 538 (2011).

[11] A. Candini, D. Klar, S. Marocchi, V. Corradini, R. Biagi, V. De Renzi, U. del Pennino, F. Troiani, V. Bellini, S. Klyatskaya, M. Ruben, K. Kummer, N.B. Brookes, H. Huang, A. Soncini, H. Wende, and M. Affronte, Spin-communication channels between Ln(III) bis-phthalocyanines molecular nanomagnets and a magnetic substrate, Sci. Rep. **6**, 21740 (2016).

[12] S. Marocchi, A. Candini, D. Klar, W. Van Den Heuvel, H. Huang, F. Troiani, V. Corradini, R. Biagi, V. De Renzi, S. Klyatskaya, K. Kummer, N.B. Brookes, M. Ruben, H. Wende, U. Del Pennino, A. Soncini, M. Affronte, and V. Bellini, Relay-Like Exchange Mechanism through a Spin Radical between $TbPc_2$ Molecules and Graphene/Ni(111) Substrates, ACS Nano **10**, 9353 (2016).

[13] A. Candini, S. Klyatskaya, M. Ruben, W. Wernsdorfer and M. Affronte, Graphene Spintronic Devices with Molecular Nanomagnets, Nanoletters **11**, 2634 (2011).

[14] M. Urdampilleta, S. Klayatskaya, M. Ruben, and W. Wernsdorfer, Magnetic Interaction Between a Radical Spin and a Single-Molecule Magnet in a Molecular Spin-Valve, ACS Nano **9**, 4458 (2015).

[15] R. Vincent, S. Klyatskaya, M. Ruben, W. Wernsdorfer, and F. Balestro, Electronic read-out of a single nuclear spin using a molecular spin transistor, Nature **488**, 357 (2012).

[16] S. Thiele, F. Balestro, R. Ballou, S. Klyatskaya, M. Ruben, and W. Wernsdorfer, Electrically driven nuclear spin resonance in single-molecule magnets, Science **344**, 1135 (2014).

[17] C. Godfrin, S. Thiele, A. Ferhat, S. Klyatskaya, M. Ruben, W. Wernsdorfer, and F. Balestro, Electrical Read-Out of a Single Spin Using an Exchange-Coupled Quantum Dot, ACS Nano **11**, 3984 (2017).

[18] K.L. Trojan, W.E. Hatfield, K.D. Kepler, and M.L. Kirk, Strong exchange coupling in lanthanide bis-(phthalocyaninato) sandwich compounds, J. Appl. Phys. **69**, 6007 (1991).

[19] K.L. Trojan, J.L. Kendall, K.D. Kepler, and W.E. Hatfield, Strong exchange coupling between the lanthanide ions and the phthalocyaninato ligand radical in bis(phthalocyaninato)lanthanide sandwich compounds, Inorganica Chim. Acta **198**–**200**, 795 (1992).

[20] T. Ishida, T. Nakamura, T. Kihara, and H. Nojiri, Chemical trend on the lanthanide-radical exchange coupling, Polyhedron, **136**, 149 (2017).

[21] M.L. Baker, T. Tanaka, R. Murakami, S. Ohira-Kawamura, K. Nakajima, T. Ishida, and H. Nojiri, Relationship between Torsion and Anisotropic Exchange Coupling in a Tb^{III}-Radical-Based Single-Molecule Magnet, Inorg. Chem. **54**, 5732 (2015).

[22] N. Ishikawa, M. Sugita, T. Ishikawa, S.Y. Koshihara, and Y. Kaizu, Lanthanide Double-Decker Complexes Functioning as Magnets at the Single-Molecular Level, J. Am. Chem. Soc. **125**, 8694 (2003).

[23] N. Ishikawa, M. Sugita, N. Tanaka, T. Ishikawa, S.Y. Koshihara, and Y. Kaizu, Upward Temperature Shift of the Intrinsic Phase Lag of the Magnetization of Bis(phthalocyaninato)terbium by Ligand Oxidation Creating an S = ½ Spin, Inorg. Chem. **43**, 5498 (2004).

[24] N. Ishikawa, M. Sugita, T. Okubo, N. Tanaka, T. Iino, Y. Kaizu, Determination of Ligand-Field Parameters and f-Electronic Structures of Double-Decker Bis(phthalocyaninato)-lanthanide Complexes, Inorg. Chem. **42**, 2440 (2003).

[25] N. Ishikawa, M. Sugita, and W. Wernsdorfer, Quantum Tunneling of Magnetization in Lanthanide Single-Molecule Magnets: Bis(phthalocyaninato)terbium and Bis(phthalo-cyaninato)dysprosium Anions, Angew. Chemie - Int. Ed. **44**, 2931 (2005).

[26] M. Shiddiq, D. Komijani, Y. Duan, A. Gaita-Ariño, E. Coronado, S. Hill, Enhancing coherence in molecular spin qubits via atomic clock transitions, Nature **531**, 348-351 (2016).

[27] F. Branzoli, P. Carretta, M. Filibian, M.J. Graf, S. Klyatskaya, M. Ruben, F. Coneri, and P. Dhakal, Spin and charge dynamics in $[TbPc_2]^0$ and $[DyPc_2]^0$ single-molecule magnets, Phys. Rev. B **82**, 134401 (2010).

[28] A. Hassan, L. Pardi, J. Krzystek, A. Sienkiewicz, P. Goy, M. Rohrer, and L.-C. Brunel, Ultrawide Band Multifrequency High-Field EMR Technique: A Methodology for Increasing Spectroscopic Information, J. Magn. Reson. **142**, 300 (2000).

[29] M. Mola, S. Hill, P. Goy, and M. Gross, Instrumentation for millimeter-wave magnetoelectrodynamic investigations of low-dimensional conductors and superconductors, Rev. Sci. Instrum. **71**, 186 (2000).

[30] S. Takahashi and S. Hill, Rotating cavity for high-field angle-dependent microwave spectroscopy of low-dimensional conductors and magnets, Rev. Sci. Instrum. **76**, 23114 (2005).

[31] S. Stoll and A. Schweiger, EasySpin, a comprehensive software package for spectral simulation and analysis in EPR, J. Magn. Reson. **178**, 42 (2006).

[32] See Supplemental Material at [URL will be inserted by publisher] for crystal structures in CIF format.

[33] C. Loosli, S.-X. Liu, A. Neels, G. Labat, and S. Decurtins, Crystal structures of tetrabutylammonium bis(phthalocyaninato)terbium(III) methanol solvate hydrate (1:1:3/2), $[N(C_4H_9)_4]$ $[Tb(C_8H_4N_2)_2]$ · CH_3OH ·$3/2H_2O$, and tetrabutylammonium bis(phthalocyaninato)dyspiosium(III) methanol solvate hydrate (1:1:1), $[N(C_4H_9)_4]$ $[Dy(C_8H_4N_2)_2$ · CH_3OH ·H_2O, Zeitschrift Für Krist. -New Cryst. Struct. **221**, 135 (2006).

[34] H. A. Kramers, General theory of paramagnetic rotation in crystals, Proc. Amsterdam Acad. **33**, 959 (1930).

[35] S. M. Winter, S. Hill and R. T. Oakley, Magnetic Ordering and Anisotropy in Heavy Atom Radicals, J. Am. Chem. Soc. **137**, 3720 (2015).

[36] S. M. Winter, R. T. Oakley, A. Kovalev, S. Hill, Spin-orbit effects in heavy-atom organic radical ferromagnets, Phys. Rev. B **85**, 094430 (2012).

[37] K.W.H. Stevens, Matrix Elements and Operator Equivalents Connected with the Magnetic Properties of Rare Earth Ions, Proc. Phys. Soc. Sect. A **65**, 209 (1952).

[38] S. Ghosh, S. Datta, L. Friend, S. Cardona-Serra, A. Gaita-Ariño, E. Coronado, S. Hill, Multi-frequency EPR studies of a mononuclear holmium single-molecule magnet based on the polyoxometalate $[Ho^{III}(W_5O_{18})_2]^{9-}$, Dalton Trans. **41**, 13697 (2012).

[39] H. Huang, W. Van den Heuvel, A. Soncini, Ab initio multi-reference investigation of the exchange coupling between 4f-electrons and \pi-radical in $[LnPc_2]^0$ molecules, in preparation.

[40] M. Damjanovic, T. Morita, K. Katoh, M. Yamashita, and M. Enders, Ligand π-Radical Interaction with f-Shell Unpaired Electrons in Phthalocyaninato–Lanthanoid Single-Molecule Magnets: A Solution NMR Spectroscopic and DFT Study, Chem. - A Eur. J. **21**, 14421 (2015).

[41] F. Branzoli, P. Carretta, M. Filibian, S. Klyatskaya, and M. Ruben, Low-energy spin dynamics in the $[YPc_2]^0$ S=1/2 antiferromagnetic chain, Phys. Rev. B **83**, 174419 (2011).

[42] A. Ghirri, M. Affronte, unpublished.